magnetism

MDPI

Article

Practical Study of Mixed-Core High Frequency Power Transformer

Arun Kumar Paul

Research and Development, M/S. Electronics Devices Worldwide Pvt. Ltd., 22 Mistry Industrial Estate, Cross Road A, Andheri East, Mumbai 400093, India; arunp26@iitbombay.org

Abstract: The design of medium- to high-frequency power electronics transformer aims not only to minimize the power loss in the windings and the core, but its heat removal features should also allow optimal use of both core and copper. The heat removal feature (e.g., thermal conduction) of a transformer is complex because there exist multiple loss centers. The bulk of total power loss is concentrated around a small segment of the core assembly where windings are overlaid. The primary winding is most constrained thermally. For superior use of core and copper, the temperature rise in different segments of the transformer should be well below their respective safe operating limits. In practice, cores of same soft-magnetic materials are traditionally used. To achieve superior temperature profile and for better long-term performance, this article proposes to use the mixed-core configuration. The new core(s) would replace the parent ones from the segment where windings are laid. The characteristic features of new cores would share increased burden of heat removal from the transformer. To obtain the qualitative insight of magnetic and thermal performance, the proposed mixed-core transformer would be thoroughly validated practically in two different high-power applications. In the first case, the core is always energized to its rated value, and in the second one, windings are always energized at respective rated current capacity.

Keywords: hot spot temperature; mixed-core magnetic circuit; power electronics systems; power electronic transformer (PET); soft magnetic materials

Citation: Paul, A.K. Practical Study of Mixed-Core High Frequency Power Transformer. *Magnetism* **2022**, 2, 306–327. https://doi.org/10.3390/magnetism2030022

Academic Editors: Roberto Zivieri, Jianguo Zhu and Gerardo F. Goya

Received: 13 May 2022
Accepted: 19 August 2022
Published: 1 September 2022

Publisher's Note: MDPI stays neutral with regard to jurisdictional claims in published maps and institutional affiliations.

1. Introduction

Power electronics converters [1] are used to ensure efficient handling of electrical energy where, as shown in Figure 1, power electronic transformer (PET) is an integral part [2–7]. Though it is a passive component, its role in power converters is immense. Apart from mandatory safety isolation, a PET could be used either for voltage [8] or current multiplication [4] to match the load characteristics of applications. Depending upon the topology of power converter used, additionally, it is often used to perform certain assisting roles in different soft-switched inverter operations [9–11]. The PET is used for instantaneous power transfer, and it should be efficient and compact. Due to the availability of a wide range of soft magnetic materials [12,13] in different geometries as well as of copper conductors (litz wires and copper foils) [14], the process of design optimization of a PET is now elaborate. For optimal design of a PET, the following aspects need to be looked into:

1. The power loss characteristics and its distribution in core and copper [15–21].
2. The distribution of steady state temperature in different parts of the core and copper windings [3,21].
3. The influence of soft magnetic materials of suitable geometry [13] as well as that of copper conductors.
4. The leakage inductance [11,22].
5. The prospect of static and dynamic DC bias in the PET [8,17], etc.

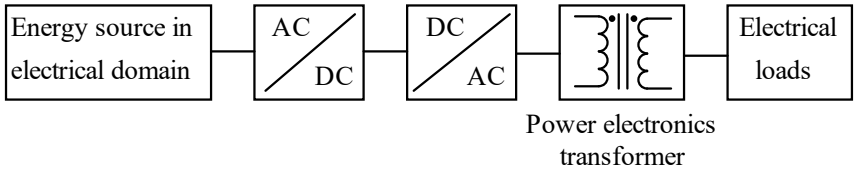

Figure 1. Arrangement of a basic power electronics system.

One typical 2-winding PET is shown in Figure 2. Its design optimization involves optimal use of core and copper; it is possible if both the core and copper losses are minimized. The copper loss P_{cu} depends on the current density of conductors, the impact of proximity effects on the resistance values of primary and secondary conductors, winding configuration and the construction of conductors [14,23]. On the other hand, the core loss P_{core} depends on the properties of the core material, peak operating flux density B_m, the excitation frequency f_s, the waveform pattern and the core temperature [18,19,24,25]. Thirdly, the design also involves devising a thermal circuit so that the temperature rise in core, copper and insulation are not only within the respective safe operating limit, but there should also be increased uniformity of maximum temperature rise in different parts of windings as well as in the core. Ensuring near-uniform temperature rise is complex because the distribution of power loss in the core is not uniform and so is the case for windings. Moreover, the thermal behavior of each circuit is also different. Ideally, for the design of the thermal circuit for heat removal, the average flux density per cycle is considered to be zero where the core loss is decided by the values of B_m and f_s; it is true when the DC bias in core is absent [17]. The presence of DC bias could adversely affect the performance of the PET in several ways. Primarily, the core loss increases significantly under DC bias; it could work as a hindrance to draw any comparative statement on performance among different PETs. Secondly, depending upon the DC bias capacity of the magnetic circuit, there could be core saturation that affects the performance of the power controller. The DC bias capacity of the magnetic circuit is poor for zero-gap magnetic circuit using high permeability materials (e.g., toroidal core using nanocrystalline materials). The DC bias could be static [26] or dynamic [27,28].

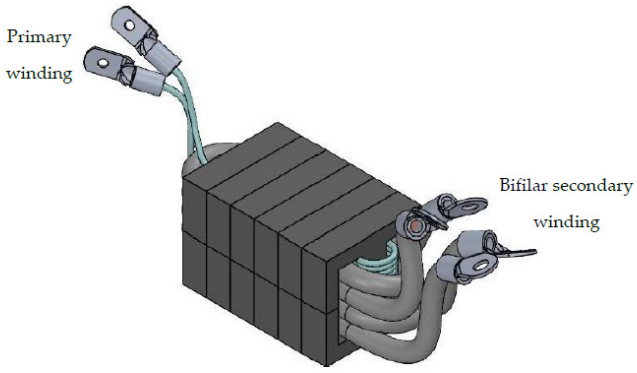

Figure 2. Typical power transformer using EE or UU cores.

Except in a few applications [8] where certain leakage inductance is desired, the design of PET necessitates that the two windings are overlaid on a small segment of the core volume [29]. Therefore, the bulk of its total power loss is concentrated around a small core volume (e.g., the central limb of Figure 2). Removal of such concentrated heat loss is a complex task. It would decide the operating limits of the core and the windings [21]. Large, concentrated power loss along with the constrained heat removal features of core and windings would result nonuniform temperature rise [3]. The respective value of maximum temperature rise would decide the capacity of core and windings. It forces the core to operate at reduced flux density because the maximum permissible operating temperature of core is less than that of copper or its insulation. It would affect the power density of the

PET. To get the desired flux level, several cores are integrated. Until recently, for medium- to high-frequency PETs, ferrites have been prominently used to build the magnetic circuit. As shown in Table 1, for ferrites, the heat removal by thermal conduction is not attractive where the prospect of creation of hot spot is comparatively large [20]. The safe operating temperature range of ferrites is also not large and several of its parameters are sensitive to temperature [13]. Therefore, cores are usually integrated to achieve multiple goals, e.g., to meet the desired flux level, to have improved thermal conduction features to distribute the core loss over larger core surface area, to reduce the number of turns and layers in the windings, etc.

Table 1. Comparison on basic parameters of a few soft magnetic materials for transformer.

Core Material	Si-Steel	Ferrite	Amorphous	Nanocrystalline
Thermal conductivity K, °C/mK	18.6	≤5	10	10
Loss density (W/kg) at 0.1 T, 20 kHz	20.0	1.9	4.7	0.9
Loss density (kW/m^3) at 0.1 T, 20 kHz	150	9.1	34	6.6
Relative permeability μ_r	900	2200	15,000	15,000
Maximum operating temperature, °C	150	100	150	120–150
Saturation flux density B_{sat} at 25 °C	1.8	4.9	1.56	1.23
Curie Temperature, °C	770	230	415	570

As detailed in [3], the temperature rise in various segments of core and copper is different; the safe operating temperature limit of each component of a PET could as well be different. For any power electronic component, for example, the differential value between its limiting temperature and maximum (hot spot) operating temperature would decide its utility as well as the service life [30]. The prospect of creation of hot spot temperature in copper is high on winding close to the core. The temperature of core is also maximum there [3]. The value of thermal conductivity K of core could play an important role in controlling the temperature distribution because, as shown in Figure 2, a major part of core assembly remains exposed to the surrounding environment. The bulk of power loss in a PET is concentrated around a small part of the core where primary and secondary windings are overlaid. Traditionally, to share the magnetic burden (flux density, core loss) equally, several cores of a similar type have been used to integrate the flux in the magnetic circuit and reduce the core loss density. Laterally, it would reduce the thermal resistance of the magnetic circuit. Often, for parametric matching dynamically, the. same batch code of cores has been strongly recommended. Now, wide-range soft magnetic materials possessing different parametric values are available. To improve the utility of a PET, can different core materials [12,13,25,31,32] be integrated in the magnetic circuit? What could be their characteristic features for integration in series or parallel configuration in a magnetic circuit to reduce either the power loss and/or to improve the thermal behavior of the PET?

The inspiration for this experiment-driven research has been the work reported in [3]. Using finite element analysis (FEA) and validated by requisite practical demonstration, it could correctly estimate the temperature distribution in different segments of core and copper. With the aim to improve the performance of PET, this article proposes, with detailed practical demonstration, to integrate different soft magnetic materials into the magnetic circuit. Here, an improved thermal conductivity and/or reduced loss density of the new core placed in a zone of high power loss is aimed to aid the cooling of regions of maximum heat generation. The structure of the article is organized as follows: Section 2 details the

features of PETs for two different characteristics applications—one used for voltage ratio and the other for current multiplication. It also discusses their design issues. Section 3 details the different perspectives of two types of mixed-core configuration suitable for two different applications. To take care of important issues such as the magnetic compatibility, etc., it also introduces application specific suitability factor for integrating different soft magnetic materials into the core. Finally, Section 4 details the practical validation of mixed-core, air-cooled transformers for two different application domains.

2. Power Electronics Transformer for Divergent Load Characteristics

Any new idea needs to be validated in different application domains. A PET is used to make the load compatible to the source; it could be achieved in several ways. A PET could be part of power transfer in PWM controlled full-bridge DC−DC converters (FBDC) [21,33], resonant converters [6,34] or for feeding a resonant tank circuit [4]. The nature of waveforms of current and voltage could change in applications. The PET could be used for voltage ratio where, at zero output power, the current in windings could be zero, or it could be used for current ratio where its primary voltage is decided by the load. In the first case, the magnetic circuit could remain loaded and the value of copper loss P_{cu} could be zero at no load. In the second case, irrespective of the magnitude of the delivered power, the windings always draw the set current. The value of the core loss P_{core} is negligible at zero power.

Achieving optimum power density of a PET is a major design goal [35]. It depends on the total power loss and the design of thermal circuit. The PET is said to be thermally loaded to its capacity when the rated power, say, P_{PET}, is delivered to the load. Traditionally, the area product $A_{\mathrm{w}}A_{\mathrm{c}}$ in Equation (1) is used to define the extent of optimization of a PET. At a particular frequency f_{s}, it suggests a large value of B_{m} in core as well as the current density J in copper windings, as given below,

$$A_{\mathrm{w}}A_{\mathrm{c}} \propto \frac{P_{\mathrm{PET}}}{B_{\mathrm{m}}J} \tag{1}$$

The expression of B_{m} for a square wave input voltage V_{in} is,

$$B_{\mathrm{m}} = \frac{V_{\mathrm{in}}}{4n_{\mathrm{p}}A_{\mathrm{c}}f_s} \tag{2}$$

A_{w} is the window area, A_{c} is the core area and n_{p} is the number of primary turns.

For effective use of a PET, its core loss P_{core} [18] and copper loss P_{cu} [23] need to be calculated accurately. For sinusoidal primary voltage, the Steinmetz equation [16] is used to calculate the value of P_{core}; its parameters are mostly mentioned in core datasheet. However, in high-frequency applications, the primary voltage is rarely sinusoidal. Using the same Steinmetz parameters, the improved generalized Steinmetz equation (iGSE) is used to calculate P_{core} for any input voltage waveform [17,19]. Using the iGSE, the expression of P_{core} with square wave excitation is,

$$P_{\mathrm{core}} = W_{\mathrm{c}}K_I 2^{(\alpha+\beta)} f_s^{\propto} B_m^{\beta} d_{\mathrm{pwm}}^{(1-\alpha)} \tag{3}$$

where $K_I = \frac{K_S}{2^{(\beta+1)}\pi^{(\alpha-1)}\left(0.2761+\frac{1.7061}{\alpha+1.354}\right)}$.

K_S, α and β are Steinmetz parameters, d_{pwm} is duty cycle of square wave input and W_{c} is the core weight. For pure square wave input (d_{pwm}: 1.0), Equation (3) may be modified to,

$$P_{\mathrm{core}} = W_{\mathrm{c}}K_{S1}f_s^{\propto}B_m^{\beta}, \quad \text{where,} \quad K_{S1} = K_I 2^{(\alpha+\beta)} \tag{4}$$

The expressions of $P_{\mathrm{cu}} = P_{\mathrm{pri}} + P_{\mathrm{sec}}$ in primary (P_{pri}) and secondary (P_{sec}) windings are,

$$P_{\mathrm{pri}} = F_1 r_{\mathrm{dc1}} i_{\mathrm{p}}^2 \text{ and } P_{\mathrm{sec}} = F_2 i_{\mathrm{s}}^2 r_{\mathrm{dc2}} \tag{5}$$

F_1 and F_2 are the ac resistance factors, i_p and i_s are the primary and the secondary current, respectively, and r_{dc1} and r_{dc2} are their respective dc resistance values. Both F_1 and F_2 depend on several factors such as skin and proximity effects where proper choice of copper conductors (litz wire or thin foil) and layout of windings are important [23].

The popular geometry of the magnetic circuit could be based on any of EE, UU or CC as shown in Figure 3a, or zero-gap toroidal shaped cores of Figure 3b. The dynamic profile of the input voltage V_{in} decides the value of B_m in core; it depends on the power controller and the characteristics of the connected load. Depending upon the value of B_m, the magnetic circuit could face nonlinearity as well as the magnetic saturation. Here, two application types are considered where the dynamics of V_{in} or B_m are completely different.

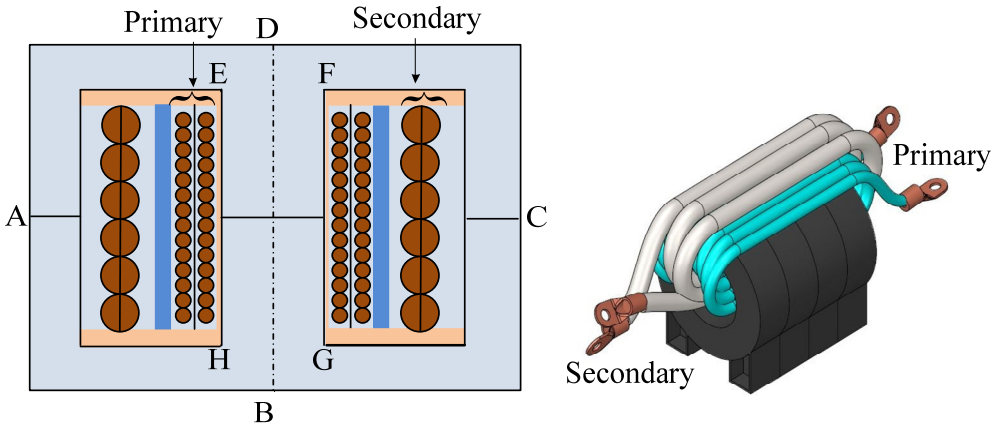

Figure 3. Popular arrangements of PET where magnetic circuit is configured in (**a**) series reluctance circuit model and (**b**) parallel reluctance circuit model.

2.1. PET for Full-Bridge DC−DC Converter (FBDC)

One typical circuit of FBDC is shown in Figure 4. Here, the magnitude of output current depends on the power drawn by the applied load at voltage V_L and its effective resistance, e.g., battery charging [11], arc welding [33], etc. Even at zero load current the cores could be fully loaded. For a nonlinear load (e.g., welding arc), the dynamic control of DC current I_a would decide the value of V_{in} or B_m through dynamic change in d_{pwm}, such as,

$$\frac{d}{dt}(I_a) = \frac{1}{L_1}(k_1 u - V_L) = \frac{1}{L_1}\left(\frac{V_{DC}}{n} d_{pwm} - V_L\right) = \frac{1}{L_1}\left(\frac{V_{in}}{n} - V_L\right) \quad (6)$$

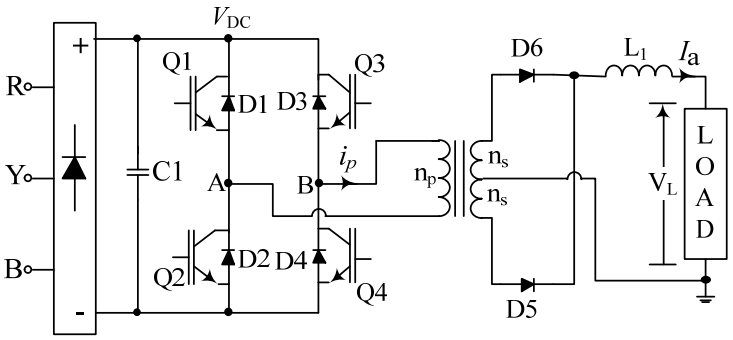

Figure 4. Typical power circuit of full-bridge DC−DC converter.

V_{DC} is the supply voltage, $n = n_p/n_s$ is the ratio of primary (n_p) to secondary (n_s) turns, k_1 is constant and the control $u = f(e)$ is used to ensure zero current error. The transient disturbance in the arc welding process is large [28].

The permissible value of J in windings would be decided by several factors such as values of F_1, F_2 and d_{pwm}. For the arrangement of secondary side rectifier of Figure 4, the primary current i_{p} and the current i_{s} in each bifilar secondary could be expressed as,

$$i_p = \frac{I_a}{n}\sqrt{d_{\text{pwm}}} \text{ and } i_s = \sqrt{\frac{1}{2}}I_a \tag{7}$$

If care is not taken, there could be error in P_{core} because the core in FBDC often faces both the static or dynamic DC bias. The static DC bias could be compensated by a simple approach [26]. The dynamic DC bias [27,28] in core would depend on how the control u (or d_{pwm}) reacts to ripple in steady state error as well as the load transients. The DC bias is more prominent when the loop gains are large where the ripple in I_{a} becomes transparent in control input u [28]. Under DC bias conditions, the values of Steinmetz parameters drifts.

2.2. PET for Series Resonant Induction Heating Equipment

The characteristics of the connected load to PET as well as its associated dynamics is quite different in induction heating. Here, the coil head L4 is kept energized with rated current i_{L} at the frequency decided by the tank circuit parameters L4 and Cr. The coil facilitates the power transfer when a metallic object is taken close to the coil. For a noncontact mode of power transfer, normally, the coil current i_{L} is kept large. To reduce the stress on primary side components, as shown in Figure 5, the induction heating transformer (IHT) is used to step up the inverter current. The value of P_{cu} is always at its rated value. The loading of its magnetic circuit and hence the core loss P_{core} depends on the power P_{OUT} drawn through L4; it depends on multiple parameters, such as,

$$P_{\text{OUT}} = K_c L_4 i_L^2 f_s = i_L^2 R_{eq} \tag{8}$$

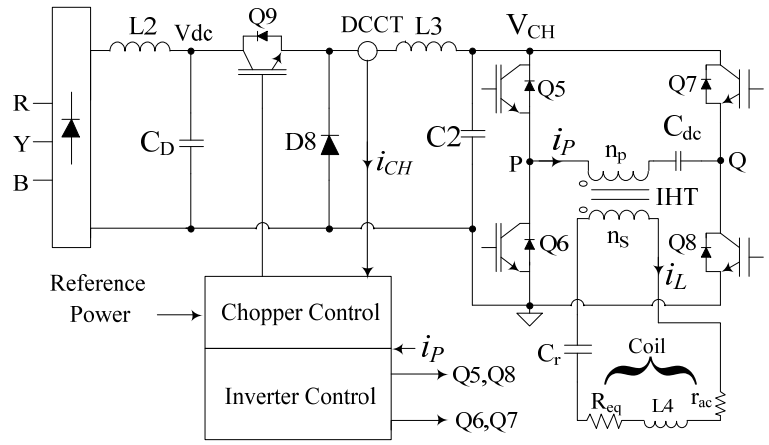

Figure 5. The power circuit for a series resonant induction heating controller.

L4 is the inductance value of coil, i_{L} is the coil current, f_{s} is frequency of i_{L} and the parameter K_{c} depends on coupling between the coil and the load. R_{eq} represents the effective load resistance reflected in the tank circuit.

The input voltage to IHT is a square wave $(d_{\text{pwm}} = 1)$, but the current in both the windings are pure sinusoidal. The DC blocking capacitor C_{dc} is connected to eliminate any static DC bias present in the core. Zero voltage switching (ZVS) condition of switches Q5–Q8 is inherently achieved because the phase-locked loop (PLL) ensures f_{s} at slightly higher than the resonant frequency $f_r = 1/2\pi\sqrt{L_4 C_r}$. Plus, the buck converter controls the input voltage V_{in} to achieve near-zero current switching of Q5–Q8. Under ZVZCS condition, the inverter input voltage V_{CH} or the primary voltage of IHT could be approximated as,

$$V_{\text{CH}} \approx V_{\text{in}} \approx 0.787n\left(r_{\text{ac}} + R_{\text{eq}}\right)|i_L| \tag{9}$$

where r_{ac} is the ac resistance of L4 and n is the turns ratio of IHT. At no load, the value of B_m is negligible because the value of $V_{in} \approx 0.787 n r_{ac} |i_L|$ is small. The change in load of IHT, i.e., the change in R_{eq} is never abrupt. Its value increases when a job is brought close to the coil (i.e., when more power is drawn through L4), and decreases gradually either near the Curie point or when the job is taken away from the coil head mechanically. They ensure that the dynamic change in B_m is also not abrupt. Moreover, the response time of the buck chopper decides the dynamics of V_{in}. Therefore, the prospect of dynamic DC bias in IHT would be small. Furthermore, the slow dynamic DC bias in the core, if any, could be effectively tackled in the PLL loop [36].

The design of IHT involves deciding on the values of n_p and n_s; selecting a core material of suitable geometry to afford optimal values of B_m and J. In ZVZCS conditions, the value of n would be maximum at n_{max} because the load behaves as resistive,

$$n = n_{max} = \frac{n_p}{n_s(\min)} = 1.27 \frac{V_{CH(max)}}{(r_{ac} + R_{eq})|i_L|} \approx 1.27 \frac{V_{DC}}{(r_{ac} + R_{eq})|i_L|} \tag{10}$$

At $n = n_{max}$, the current is minimum in the primary winding and the length of conductor used in the secondary is also minimized, and together they help minimize P_{cu}. Large values of B_{sat} and small values of P_c of nanocrystalline cores would allow optimal choice of n_p as well.

Secondly, for efficient transfer of power $P_{OUT} = i_L^2 R_{eq}$, tracking of f_r should be accurate. The value of R_{eq} would be more at higher values of f_r [37]. When L4 is loaded, its inductance value drifts down to, say, L_{eq}; then, the corresponding value of f_r is,

$$f_r = \frac{1}{2\pi\sqrt{(L_{lk} + L_{eq})C_r}} \approx f_s \tag{11}$$

L_{lk} is leakage inductance of IHT; its large value would be a hindrance to effective power transfer [37]. The value of L_{lk} is small for high-permeability ungapped toroidal cores.

Thirdly, the primary current i_{pri} consists of triangular wave magnetizing current with peak at I_m plus the reflected sinusoidal coil current i_L. For minimum phase error between V_{pri} and i_{pri} of IHT, the value of I_m should be small; it is expressed as,

$$I_m = \frac{l_m B_m}{\mu_0 \mu_r n_p} \tag{12}$$

where l_m is the mean core length. A large value of μ_r is needed for small value of I_m and n_p.

For IHT, the high-permeability nanocrystalline material-based ungapped toroidal cores (shown in Figure 3b) would be preferred [15,38–40], particularly because the DC bias in the core is negligible. Laterally, these cores would ensure small values of I_m and L_{lk} and also the minimum of number of turns where the value of B_m would be large.

3. Mixed-Core Transformer Configuration

It was clear in Sections 2.1 and 2.2 that the type of application or load characteristics could influence the design of PET. The nature of loading of magnetic circuit, in particular, could vary in applications, e.g., the value of P_{core} could be fixed and that of P_{cu} would be decided by the load. Along with reducing the core and the copper losses, the optimization process involves design of a thermal circuit to ensure near-uniform temperature rise in core and also in copper so that the PET is enabled to deliver more power. Due to multiple loss centers, the thermal circuit of the core and windings are coupled. For the magnetic circuit, the distribution of heat and its removal by thermal convection could be improved if the value of K as well as that of the surface area of core are increased. To have requisite flux $A_c B_m$, several cores are integrated. Often, for magnetic compatibility, cores of the same material with the same batch code are preferred. It is important to find whether such arrangement is best suitable for efficient heat removal, both from the core assembly as well

as from the windings. On the other hand, can some other combinations, such as the hybrid core configuration, manage the heat loss or the thermal issues better?

3.1. Thermal Behavior of Power Electronic Transformer

As shown in Equations (3) and (5), the values of P_{core} and P_{cu}, respectively, increase exponentially with B_m and with J^2. The design optimization of a PET is complex because the layout of the windings and thermal behavior of the PET often contradict. As shown in Figure 3a,b, two windings are overlaid for better magnetic coupling and also for reduced eddy current loss in core [29]. Such arrangement needs good heat removal features because the bulk of total power loss ($P_{tot} = P_{core} + P_{cu}$) is concentrated around a small core segment where the secondary winding is laid above the primary. Removing the heat loss from the multilayered primary winding is difficult because there exists insulation on either side of each layer and also between the windings. The prospect of creation of hot spot is more in the primary [3]. Furthermore, due to the increased impact of the proximity effect, the value of P_{cu} would be more in multilayered winding. Though the thermal circuit of PET is coupled in a complex manner, the limiting values of B_m and J would be decided by the effectiveness of the thermal circuit [3,39,40]. With given loss, the safe operating temperature for the core would depend on the soft magnetic materials and that for copper would be on the insulation of litz wire strands as well as that placed between the layers.

Due to the complex nature of the thermal circuit, there exist multiple heat conduction channels with different heat transfer coefficients, and they are mostly coupled [3]. The directions of heat flow would be decided by the location of the hot spot temperature T_{hs} of the PET; it could be decided by the temperature differential $\Delta T = T_{hs} - T_{amb}$, such as,

$$T_{hs} - T_{amb} = \Delta T = R_{PET}(P_{core} + P_{cu}) \tag{13}$$

$R_{PET} = R_{th} + R_{conv}$ is the effective thermal resistance of the PET and T_{amb} is the ambient temperature. R_{PET} mostly consists of thermal conduction (R_{th}) and thermal convection (R_{conv}). Though it plays certain role, the heat transfer by radiation is ignored here. For compact design of PET, apart from reducing the total loss P_{tot}, the value of ΔT should be minimum. Large surface area of the core and the secondary winding are available for heat transfer. The major part of P_{tot} is removed by thermal convection [21,41,42] where the speed of the moving medium would play a significant role. The expressions of conductive and convective thermal resistances are,

$$R_{cond} = \frac{1}{h_{cond} A_{cond}} \text{ and } R_{conv} = \frac{1}{h_{conv} A_{conv}} \tag{14}$$

A_{cond} and A_{conv}, respectively, are areas available for conduction and convection and h_{cond} and h_{conv} are corresponding heat transfer coefficients. The value of h_{conv} depends on thermal conductivity of the attached medium and also on its speed where fan cooling improves its value significantly. Backed by practical validation, the finite element method (FEM) was extensively used to establish reasons behind the formation of hot spots in core and copper in high-power transformers [3]. It was realized that the temperature rise in copper was alarming on multilayer winding with constrained heat transfer features, e.g., the primary winding of Figure 3a. In multilayer winding, a significant part of P_{cu} is concentrated in the internal layer of primary winding closest to the core where the proximity effect is more prominent. The hot spot temperature T_{hs} is located here; its value needs to be reduced. It could be made possible if a part of P_{pri} close to I-section, in particular, is channelized to the ambience through the core. Considering the heat conduction is symmetrical around the I-section of Figure 3a, the overall heat conduction circuit of half of

the PET (shown in Figure 6a), is represented in Figure 6b. The part P_{cu1} of total copper loss P_{cu} that could be channelized through the core is expressed as [41],

$$P_{cu1} = P_{cu}\frac{R_w + R_{wa} - R_{ca}\frac{P_{core}}{P_{cu}}}{R_w + R_{wa} + R_{ca} + R_F} = P_{cu}f(P_{core}, R_{ca}) \quad (15)$$

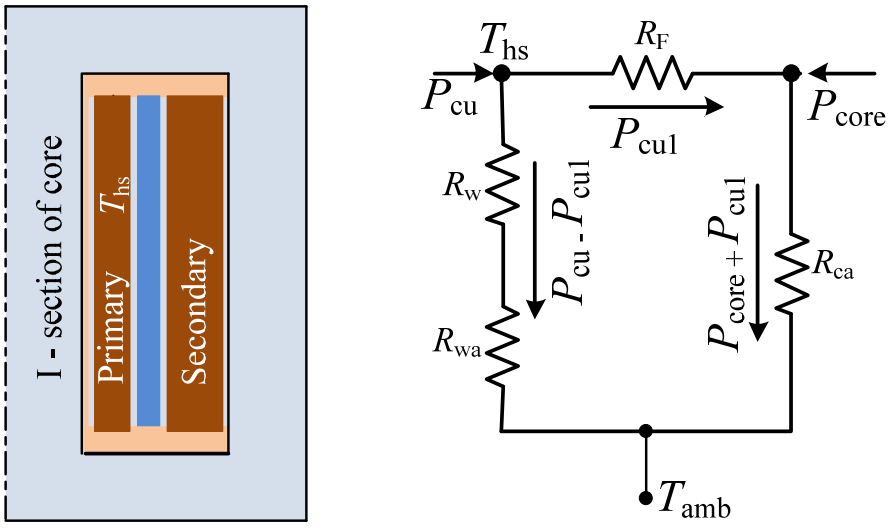

Figure 6. (**a**) Symmetrical half of PET of Figure 3a and (**b**) equivalent thermal circuit to remove heat loss.

R_w and R_{wa}, respectively, are the conductive and the convective resistance of the winding, and R_F and R_{ca}, respectively, are the effective thermal resistance of the coil former and the core. It is clear that more heat loss (i.e., P_{cu1}) would be channelized through the core if either of R_{ca} or P_{core} or together could be reduced through design or selection of suitable soft magnetic material; reduction of R_F would also play certain assisting role.

To achieve the abovementioned objective, it is proposed to use a mixed-core configuration for the magnetic circuit. It is known that a small fraction of core volume handles most of P_{tot} while the major part of its surface area is exposed to the ambience. Therefore, if that particular small section of core volume is replaced by a suitable soft magnetic material, then better heat removal feature by convection and radiation could be realized. The new core material is desired to possess following features:

1. Superior thermal conductivity.
2. Reduced core loss density.
3. Higher maximum operating temperature than the parent core.
4. The new material must be magnetically compatible.

Basic features of different soft magnetic materials are listed in Table 1.

3.2. Magnetic Compatibility of Different Types of Magnetic Circuits

For a given magneto motive force (MMF) *F*m, the magnitude of magnetic flux φ linking the windings is decided by the reluctance value R_m of its magnetic circuit. The reluctance circuits of the core assemblies of commonly used high-power PETs of Figure 3a,b could, respectively, be represented in Figure 7a,b. Traditionally, the value of loss density P_c is considered at the same value everywhere. It means, for one type of cores, the value of B_m should be same everywhere. However, in the proposed idea of using the mixed core configuration, the value of loss density could be different. The expression of flux φ linking the windings is,

$$\varphi = \frac{F_m}{R_m} \quad \text{where} \quad R_m = \frac{l_m}{\mu_0 \mu_r A_c} \quad (16)$$

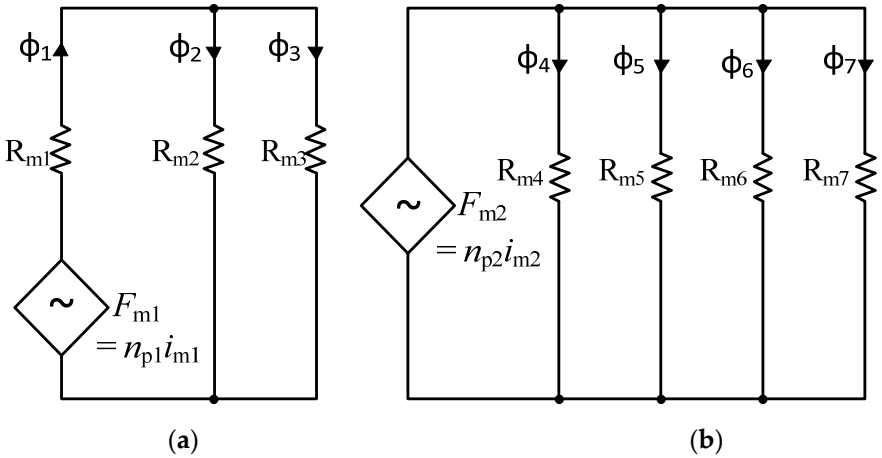

Figure 7. Reluctance circuit model of the (**a**) PET of Figure 3a and (**b**) PET of Figure 3b.

For Figure 7a, with MMF F_{m1}, the total flux $\varphi_1 = \varphi_2 + \varphi_3$ in the central limb is,

$$\text{or, } \varphi_1 = \frac{F_{m1}}{R_{\mathrm{m}}} = \frac{n_p i_{m1}}{R_{\mathrm{m}}}, \quad \text{where, } \quad R_{\mathrm{m}} = R_{\mathrm{m1}} + \frac{R_{\mathrm{m2}} R_{\mathrm{m3}}}{R_{\mathrm{m2}} + R_{\mathrm{m3}}} \tag{17}$$

It is desired to have $\varphi_2 = \varphi_3$, and it could be achieved when $R_{\mathrm{m2}} = R_{\mathrm{m3}}$ is met.

For the magnetic circuit of Figure 7b, considering the same value of reluctance in each circuit, the total flux φ in the core assembly could be expressed as,

$$\varphi = \varphi_4 + \cdots + \varphi_7 \approx 4\frac{n_{\mathrm{p2}} i_{\mathrm{m2}}}{R_{\mathrm{m4}}} \cdots \approx 4\frac{n_{\mathrm{p2}} i_{\mathrm{m2}}}{R_{\mathrm{m7}}} \tag{18}$$

where i_{m2} is the magnetizing current and n_{p2} is the number of turns at primary. Neglecting the dimensional tolerance of the cores, the dynamic value of R_{m} of each parallel path plays an important role in flux distribution. When composite core segments are used, the dynamic behavior of μ_{r} becomes critical for designing the magnetic circuit of Figure 7b. The value of μ_{r} could change differently with respect to operating value of $B_{\mathrm{m}}, f_{\mathrm{s}}$, temperature, etc.

Characteristics of Different Soft Magnetic Materials

It is clear that for the magnetic compatibility, the role of relative permeability μ_{r} is extremely important. For better thermal performance, the heat distribution (Equation (15)) should be proper, i.e., more heat needs to be transferred to the core surface area exposed to the environment. Here, both the core loss density P_{c} and the thermal conductivity K would play significant roles. The basic parameters of popular soft magnetic materials are listed in Table 1 [20]. For ferrite cores, the parametric variation with respect to temperature [13] is large. Compared to others, its Curie temperature is much lower. The reduction in B_{sat} value vs. temperature is also sharp. For integration of different core types into a magnetic circuit of PET, the value of μ_{r} at different flux density and core temperature is important. The influence of temperature on μ_{r} of different soft magnetic materials is shown in Figure 8 [43] where nanocrystalline cores appear to be parametrically robust. It is also known that, for ferrite cores, the value of μ_{r} changes significantly with flux density [4]. However, for nanocrystalline cores, as shown in Figure 9, the value of μ_{r} is mostly constant, and only at large values of B_{m} is there gradual monotonic drooping in its value. Moreover, compared to other soft magnetic materials, the core loss of nanocrystalline cores at a particular frequency is comparatively less at any flux density (shown in Figure 10). Therefore, due to the parametric robustness, small core loss density, superior thermal conductivity, higher saturation flux density and high Curie temperature, the nanocrystalline cores of proper ribbon thickness are superior candidates for mixed-core configuration. It would not disturb the behavior of the magnetic circuit. If geometry permits, Fe-based nanocrystalline cores

could ideally be suitable as flux integrators for medium- to high-frequency PETs. The drooping characteristics of μ_r, as shown in Figure 9, make these cores suitable for integration into a magnetic circuit where the MMF feeds several parallel magnetic circuits (shown in Figure 3b).

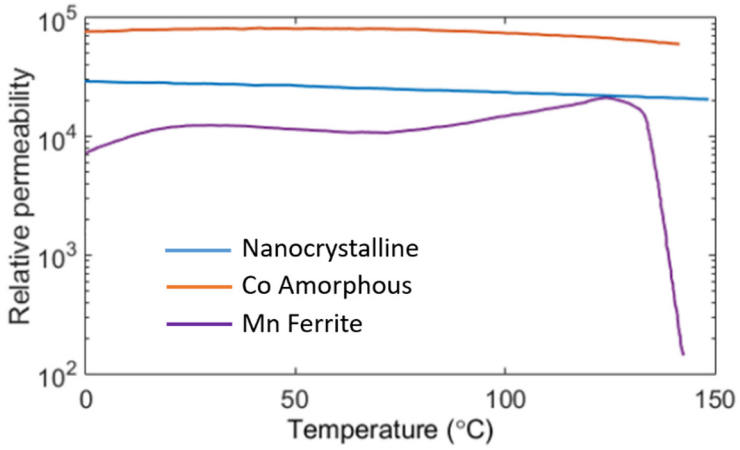

Figure 8. Behavior of relative permeability of soft magnetic materials vs. temperature [43].

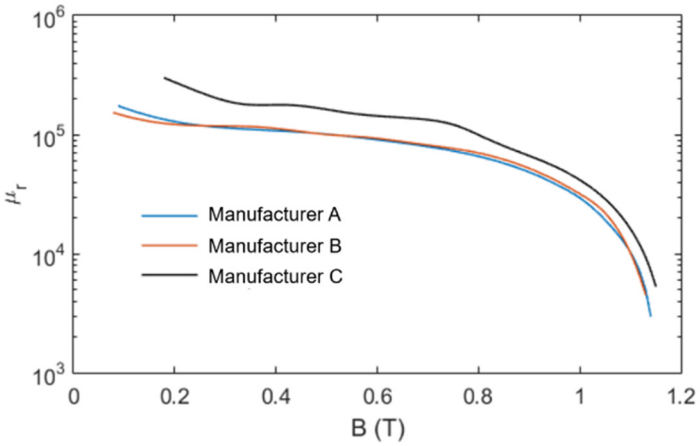

Figure 9. Permeability vs. flux density of competitive nanocrystalline cores have similar drooping characteristics.

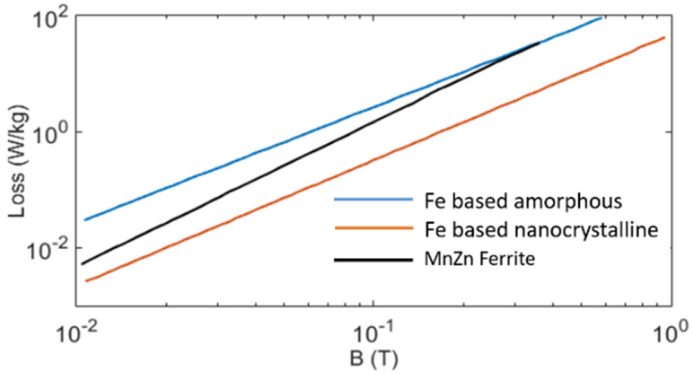

Figure 10. At a particular frequency the core loss density in nanocrystalline cores is minimum.

3.3. Figure of Merit of Mixed-Core Magnetic Circuit for Series Reluctance Model

It is known that for the PET of Figure 3a, the bulk of total power loss P_{tot} is concentrated around the central I-section EFGH. The hot spot temperature in the core and the primary

winding, in particular, would reside in and around the I-section [3]. In order to properly utilize the large surface area of core exposed to the ambient medium for thermal convection and radiation, there needs to be an improvement in spreading the heat loss in the core by thermal conduction. A higher value of thermal conductivity K of core in the I-section EFGH would help remove the concentrated heat loss to the surface area of the magnetic circuit. As detailed in Equation (15), more power loss could be channelized if,

1. The value of P_c of the I-section is small.
2. The value of K of soft magnetic material used in the I-section is more.
3. The value of thermal resistance in coil former is reduced.

The first two features could simply be achieved if the central I-section is replaced by a geometrically compatible core material (shown in Figure 11a) with superior features so that the value of ΔT (see Equation (13)) in the I-section of core is reduced. The compatibility of the new material would be based on its dynamic magnetic parameters, core loss density P_c and the value of K. From the magnetic characteristics point of view, the role of I-section is not complicated. The *Figure of Merit* of the new core material for the I-section could be gauged by a suitability parameter S_{core}(SR); it is introduced in simple form as,

$$S_{\text{core(SR)}} = \frac{K}{P_c} \text{ and, } \mu_{\text{rn}} \geq \mu_{\text{rp}} \tag{19}$$

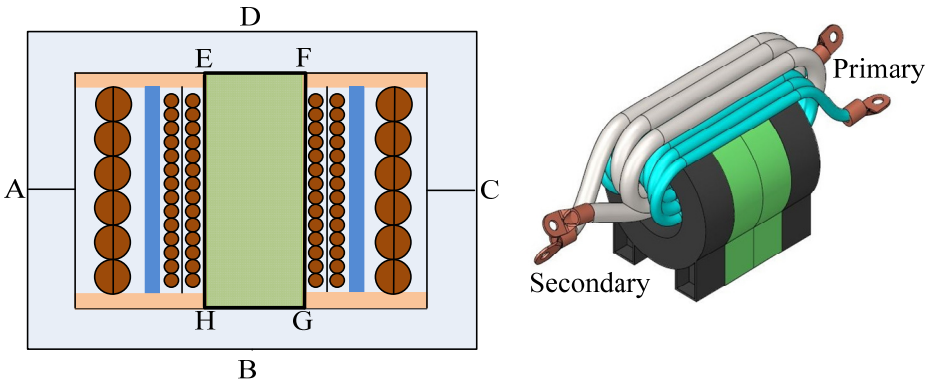

Figure 11. Mixed-core assembly is for better use of the (**a**) electrical circuit of PET, i.e., the windings, and (**b**) magnetic circuit or the core assembly.

When compared with parent material, a smaller value of P_c and the same or larger value of K would result in superior distribution of heat in core. The permeability μ_{rn} of new I-section should be around the same value as μ_{rp}, i.e., of parent material. The value of K and other relevant parameters for different core materials are listed in Table 1.

3.4. Figure of Merit of Mixed-Core for Parallelly Connected Magnetic Circuit

Multiple toroidal cores are stacked (shown in Figure 3b) to support the desired flux level in the core of IHT. It is difficult to remove the heat loss from each core uniformly. The surface area of inner cores exposed to the ambient medium is relatively much less. It could lead to differential temperature rise across the core segments. In practice, the inner cores are found to be hotter. Like the PET of Figure 11a, here as well, as shown in the arrangement of Figure 11b, the problem could be reduced if the inner cores are replaced by a superior material. For a magnetic circuit where cores are used in parallel, it is difficult to establish the desired flux density everywhere. The dynamic value of relative permeability of each core being integrated would play an important role. To find the compatibility of the

new core material for parallel reluctance model, and also to take care of sharing of flux, the suitability factor S_{core} of Equation (19) is modified to,

$$S_{\text{core(PR)}} = \frac{\mu_r(B_m)}{P_c}K, \quad \text{and for } B_{\text{m1}} > B_{\text{m2}}, \quad \mu_{r1} < \mu_{r2} \tag{20}$$

where $\mu_{\text{r}}(B_{\text{m}})$ is the value of μ_{r} of core at the operating value of B_{m}. It takes care of the distribution of flux when the condition (for $B_{\text{m1}} > B_{\text{m2}}$, $\mu_{r1} < \mu_{r2}$) is met. As shown in Figure 9, nanocrystalline cores support such characteristics. Furthermore, as shown in Figure 8, the value of μ_{r} for this core is also stable against temperature.

4. Experimental Validation of Mixed-Core Transformers

To validate the proposed idea of improving the thermal performance of a mixed-core PET, two divergent application domains were considered. In the first, to ignore any role of DC bias, the magnetic circuit was completed using two UU cores. In the second case, because the dynamics of B_{m} were sluggish, the ungapped toroidal shaped cores were assembled. In the first case, the prospect of transient DC bias was more. The magnetic circuit needed to be built with large DC bias capacity where, for large power applications, EE, UU or CC cores were suitable. On the other hand, for IHT, the prospect of transient DC bias was small. Therefore, ungapped toroidal cores with large permeability were preferred in the magnetic circuit.

4.1. Validation of Mixed-Core PET Where the Magnetic Circuit Uses UU cores

Ferrite cores in EE or UU shape are prominently used in high-power PET of Figure 3a where the central limb hosts both the windings. Due to their superior characteristics, as described in Equation (19), nanocrystalline cores would ideally be preferred for the I-section of Figure 11b. However, these ribbon-type cores are not dimensionally compatible as yet with the commonly available ferrite cores. It is difficult to match important dimensions one-to-one, e.g., the core area A_{c}, the window area A_{w}, the mean magnetic length l_{m}, etc.

It was difficult to procure I-shaped nanocrystalline cores physically or geometrically compatible to commonly used UU or EE ferrite cores. Therefore, to study the role of K and P_{c} on the thermal performance of PET, as shown in Figure 12, two mixed-core transformers (MCT) were built using different ferrite cores with different values of P_{c} and K. For core assembly, each MCT combined two different core types A and B procured from separate manufacturers. Relevant parameters of these cores are listed in Table 2.

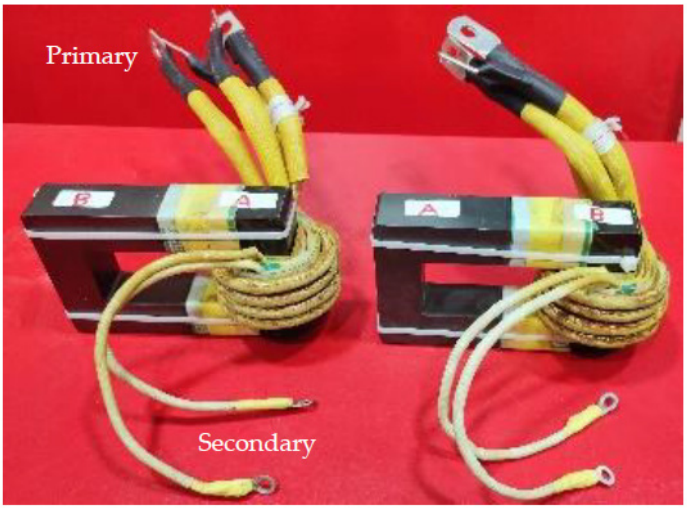

(**a**) (**b**)

Figure 12. Mixed-core transformers for FBDC where windings are overlaid on the core of material type (**a**) A for PET A and (**b**) B for PET B.

Table 2. Properties of ferrite cores type A and type B.

Core Material	Ferrite Core A		Ferrite Core B	
At temperature	25 °C	100 °C	25 °C	100 °C
Initial permeability	2500		2200	
B_{sat}, T	0.47	0.38	0.49	0.39
Curie temp., °C	>230		>210	
P_c @ 0.2 T, 25 kHz, kW/m^3	130	65	130	57
P_c @ 0.1 T, 100 kHz, kW/m^3	135	65	140	50
Thermal conductivity K, W/mK	≤4.3		5.0	

For testing of PETs A and B of Figure 12, one 20 kHz full-bridge DC−DC converter (shown in Figure 4) operating at 20 kHz was developed. The power controller is shown in Figure 13. For switching of inverter, IGBTs (Type: 2MBI075VAA-120-50) were used. The value of V_{DC} was 560 V. The value of inductor L1 was 100 µH. The winding layout of PETs A and B was similar, each had two secondary bifilar windings. To practically compare the magnetic compatibility at high flux density, the turns-ratio n_p:n_s:n_s of PETs was deliberately chosen at 24:2:2. The value of B_m at maximum value of d_{pwm} at 80% was 0.325T. Moreover, at the rated output power P_L at 4.5 kW (PWM duty cycle $d_{pwm} \approx 57\%$), the magnetic circuit would be loaded to the rated value of B_m at around 0.2 T. Each PET used one pair of UU cores, the value of A_c was 8.4 cm^2. At rated load current (I_a: 200 A) with d_{pwm} at 57%, the current density J (A/mm^2) at primary (strand dia.: 0.1 mm, 450 strands) and secondary litz wire (strand dia.: 0.1 mm, 3780 strands) conductors were 3.56 and 4.72, respectively. Due to higher value of J, the power loss in secondary conductors was more.

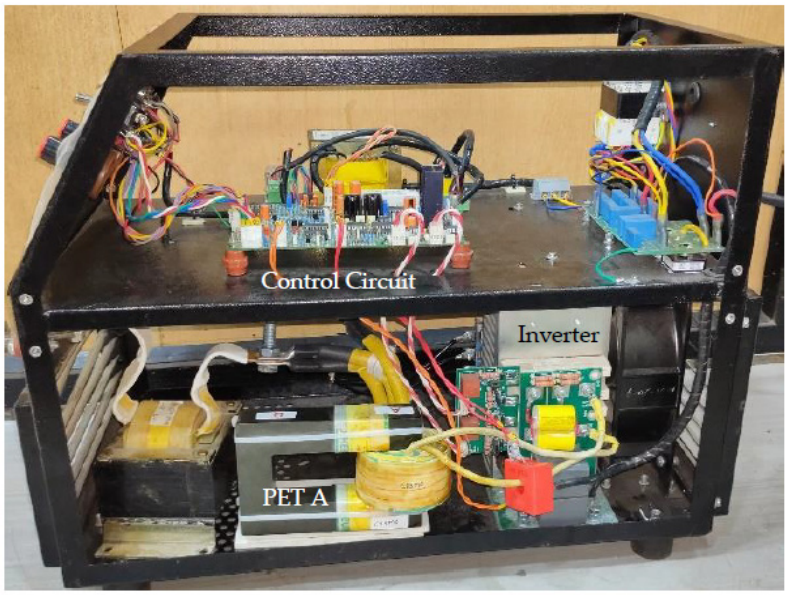

Figure 13. Prototype of a 4.5 kW DC−DC converter for performance testing of PET A and PET B.

Two sets of waveforms with an exactly similar nature of the magnetizing current i_{m1} (both secondary: open) in Figure 14a,b demonstrated that the core A and B were magnetically compatible even in the nonlinear zone of the *B*–*H* curve. At d_{pwm} of 80%, the value of B_m was deliberately kept large at 0.325 T so that the magnetic compatibility in the nonlinear zone was verified. The magnetic circuit had rated value of B_m (≈0.2 T) at designed power output.

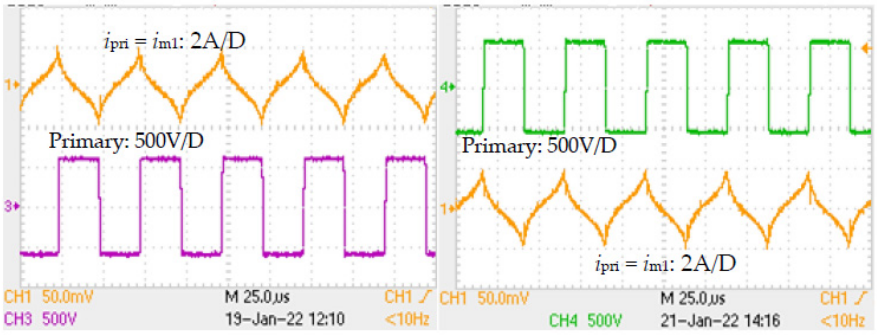

(**a**) (**b**)

Figure 14. At zero secondary current, even in nonlinear operating zone of B-H curve (B_m = 0.325 T), the behavior of the magnetic circuit of (**a**) PET A was similar to that of (**b**) PET B.

To evaluate the thermal performance comparatively, the two transformers were (resistive) load tested until the temperature in core and copper stabilized. The ambient temperature was 28 °C. The delivered power to load was 4.5 kW where the load voltage V_L was maintained at 22.5 V. At full load, the calculated value of B_m was 0.207 T. Various waveforms of the FBDC using PET A and PET B are shown in Figures 15a and 15b, respectively. Using the Fluke make 59 *Mini* IR thermometer, the temperature was recorded in each winding and also in the core segment close to the windings. The measured value of the hot spot temperature in the core and the windings of two PETs are listed in Table 3. It was clear that, compared to PET A, the temperature distribution of PET B was superior. The experimental results made it clear that the core type with lower value of P_c and/or possessing higher value of K would be more suitable for the core segment where the windings are laid. It could be stated that the situation would improve further if the I-section was replaced by a suitable nanocrystalline core material.

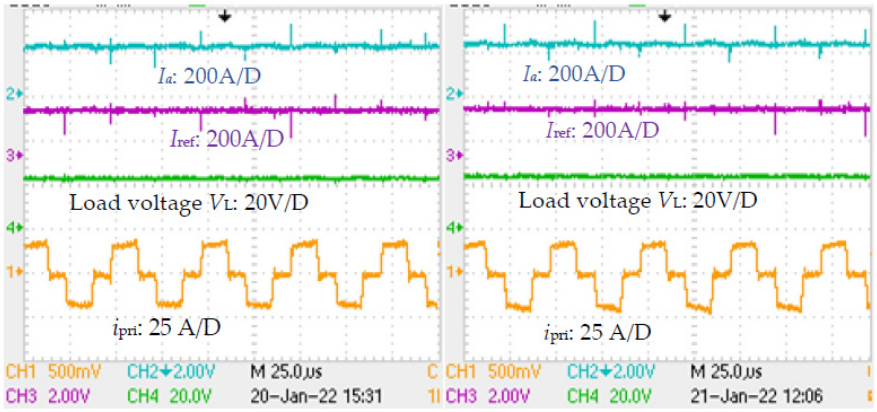

(**a**) (**b**)

Figure 15. Waveforms of FBDC controller when 200 A was drawn by the load and, in that loading condition, the magnetic circuit was loaded with B_m at 0.207 T, for both (**a**) PET A and (**b**) PET B.

Table 3. Measured hot spot temperature (°C) in core and windings (Ambient temp.: 28 °C).

Transformer	Primary	Secondary	Temperature of Core (°C)
PET A	86.9	92.8	Core A: 61.7
PET B	83.6	89.3	Core B: 57.3

The results detailed above were found to be reproducible when thermal images of PET A and PET B were captured by a camera (model: FLIR AX 5). In the captured images,

the hot spot temperature of the secondary winding (SP1), primary winding (SP2) and also in the core (SP3) for two different case studies are shown in Figure 16 (for PET A) and in Figure 17 (for PET B). It was clear that the core of reduced value of P_c and of larger value of K helped reduce the hot spot temperature of PET B. The results mostly tallied with the findings of the temperature profile obtained through the noncontact type Fluke make 59 *Mini* IR thermometer.

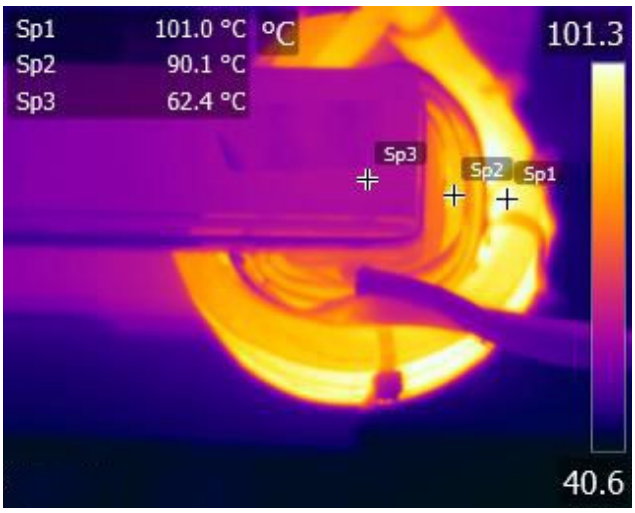

Figure 16. Temperature distribution of PET A using thermal camera (ambient temp.: 33 °C).

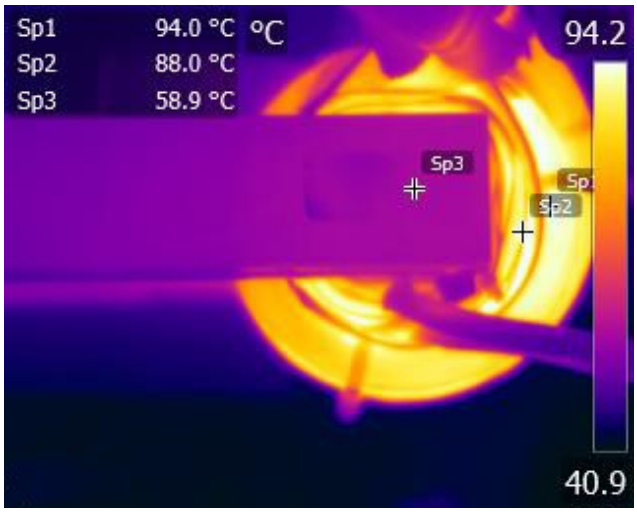

Figure 17. Temperature distribution of PET B using thermal camera (ambient temp.: 33 °C).

4.2. Validation of Mixed-Core IHT for Parallelly Connected Core Assembly

The loading pattern of the magnetic circuit of IHT is different. The value of P_{cu} is desired to be minimized because it is always at its rated value. It was analyzed in Section 2.2 that the ZVZCS topology along with using a low-loss magnetic circuit with a high effective value of μ_r and high saturation flux density B_{sat} would simultaneously minimize the copper content in IHT and also the value of P_{cu}. It requires the core to operate at a large value of B_m where cores with low loss density and high values of B_{sat} would be suitable. When both windings are placed in single layers, the impact of proximity effect on P_{cu} is minimized. Laterally, it would achieve better features for heat removal because windings are exposed to the ambient medium. For the magnetic circuit, the ungapped toroidal cores using nanocrystalline material would be a preferred choice because:

1. The value of magnetizing current would be small.

2. The value of leakage inductance would be negligible.
3. IHT does not need large DC bias capacity; transient load disturbance is small.
4. For large value of B_m (>0.25 T), ferrites are not suitable.

To practically study the usability of the proposed MCT, one induction heating controller was developed to deliver 40 kW output power. The complete experimental set up is shown in Figure 18. For comparative analysis, two transformers, i.e., the traditional single core-type IHT I and the mixed-core transformer IHT II, were designed using nanocrystalline cores. As shown in Figure 19a, in IHT I, four similar cores of, say, material type C, were stacked. Whereas in IHT II, as shown in Figure 19b, two poorly ventilated central cores were replaced by cores of different material, say, type D. The parametric details of both C and D type cores are listed in Table 4. Due to the reduced thickness of ribbons, when compared with core C, the value of P_c in core D was less. Naturally, the core D resulted superior value of S_{core}(PR) (see Equation (20)). The operating parameters of the inverter and cores are listed in Table 5. To study the magnetic compatibility, one single-turn search coil was wound on C and D cores each (shown in Figure 19b). The turns-ratio of each IHT was 8:3. For the tank circuit, the value of L4 was 52 µH and that of Cr was 3.6 µF. The inverter frequency was 12.5 kHz. With set coil current at 250 A, the value of J in primary (strand dia.: 0.1 mm, 2880 strands) and secondary (strand dia.: 0.1 mm, 2 × 3780 strands) conductors were 4.15 A/mm^2 and 4.21 A/mm^2, respectively.

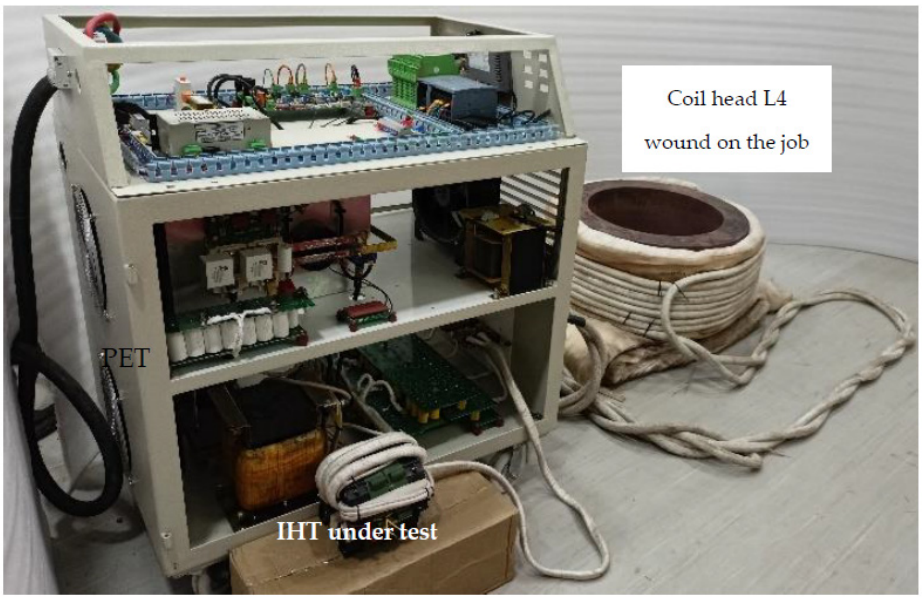

Figure 18. 40 kW induction heating controller for testing of IHTI and IHT II.

(**a**) (**b**)

Figure 19. Two 40 kW, 15 kHz transformers: (**a**) IHT I with original set of C cores and (**b**) IHT II with mixed-core configuration (C-D-D-C).

Table 4. Parameters of core *C* (black) and *D* (green).

Parameter	Core C	Core D
B_{sat} at 25 °C (130 °C), T	1.2 (1.18)	1.25 (1.21)
Initial permeability μ_r	>300 k	>300 k
K_{S1}, α, β	0.94, 1.4364, 1.638	0.22, 1.608, 1.681
Value of μ_r at B_m = 1 T	>12 k	>12 k
Ribbon thickness, µm	30	22
Area of each core, cm^2	5.25	5.62
Mean length of core, cm	29.8	29.8
P_c @0.2 T, 20 kHz, W/kg	4.98	1.82
P_c @0.6 T, 10 kHz, W/kg	11.2	3.78
Th. conductivity *K*, W/mK	10	10

Table 5. Operating parameters of IHT and core loss data.

	IHT I	IHT II
Delivered power, kW	35	
Input voltage to inverter at full load, V	450	
Inverter frequency at full load, kHz	12.5	
Core area, cm^2	21	21.74
Value of B_m in C, T	0.535	0.517
Value of B_m in D, T	-	0.517
Core loss density in each of C, W/kg	12.7	12.0
Core loss density in each of D, W/kg	-	4.21

Initially, the magnetic compatibility of cores C and D in the IHT II was tested for three different operating conditions; they are:

1. The magnetic circuit operated at maximum value of B_m when the secondary was kept open and the primary was excited with full voltage. The control circuit was disabled. The current at primary was the magnetizing current. Waveforms in Figure 21a validated that the two core types were magnetically compatible. Exactly similar nature of induced voltages in the single-turn search coils $V_{src\text{-}C}$ (core C) and $V_{src\text{-}D}$ (core D) proved that the flux density was shared appropriately.
2. The tank circuit was connected, but the power delivered through the coil head was zero. Moreover, there was a DC blocking capacitor C_{dc} of 100 µF added between primary of IHT II and the inverter output. The primary voltage was small. Here, as well, the two core types were found to be magnetically compatible (shown in Figure 21b) because even at very small flux density the readings in both the search coils were similar dynamically.
3. Magnetic compatibility of cores of IHT II was also tested when the secondary was loaded. The coil head L4 was loaded at 20 kW. The necessary waveforms are shown in Figure 20a. Here, as well, the voltage waveforms of both search coils appeared similar—in magnitude as well as in waveshape. Similar search coil voltage readings at zero secondary current as well as under loaded condition proved that cores C and D were integrated into the magnetic circuit of IHT II.

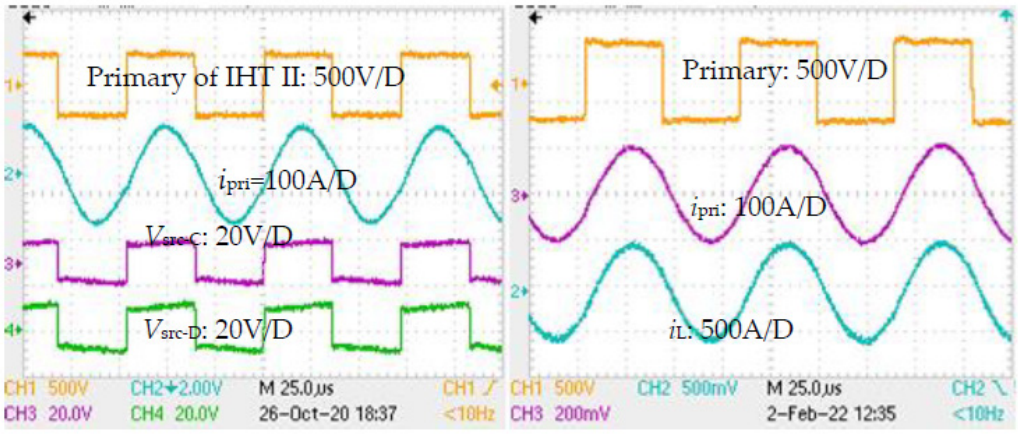

(**a**) (**b**)

Figure 20. (**a**) The magnetic compatibility of IHT II was also verified when the coil head was loaded. (**b**) Waveforms of different variables of the inverter when the IHT was loaded at 35 kW while delivering power to a section of pipe through the coil head L4.

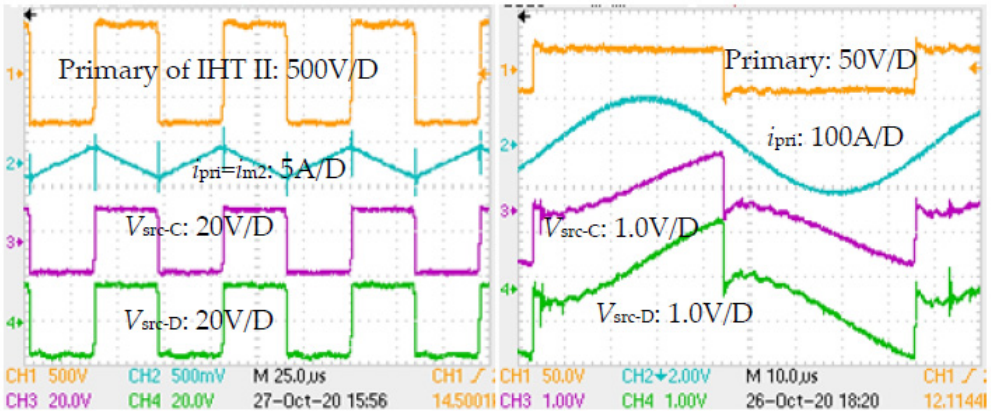

(**a**) (**b**)

Figure 21. Magnetic compatibility of C and D cores was verified through similar voltage readings in search coils wound on the respective cores, when (**a**) the secondary of IHT II was kept open, and (**b**) the DC blocking capacitor C_{dc} of 100 μF was added (shown in Figure 5) but the coil L4 was not loaded.

In order to gauge the gain of using the MCT, both IHT I and IHT II were put on a heat run test. The power drawn from the inverter was 35 kW (corresponding waveforms are shown in Figure 20b). IHTs were kept in open air under natural convection (shown in Figure 18). Each test was conducted until the steady state temperature in each core was attained. The ambient temperature was 26 °C. Using the noncontact type Fluke make 59 *Mini* IR and subsequently verified by the RTD thermometers at the end of the test, the temperature was recorded, as detailed in Figure 22, not only in each winding but also in each core segment. The measured hot spot temperature in different core and the windings of both the IHTs are shown in Figure 23. Due to the large value of K (see Table 4), the temperature distribution was found to be nearly uniform in each core segment. Moreover, compared to IHT I, temperature rise in each core of IHT II was reduced. The variation in temperature rise among different cores was also reduced. The temperature reading of internal cores with material D was much less when compared with that of IHT I. It essentially demonstrated that the power handling capacity of the MCT could be upgraded, and its power density could as well be increased.

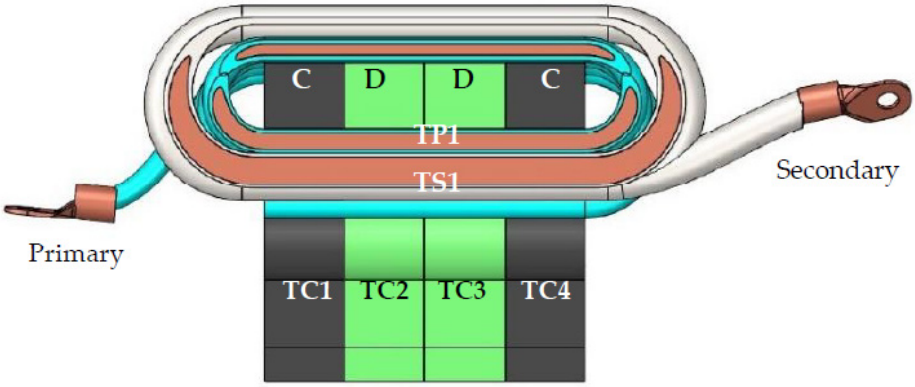

Figure 22. Sectional view of 40 kW transformer in mixed-core (core C and D) configuration.

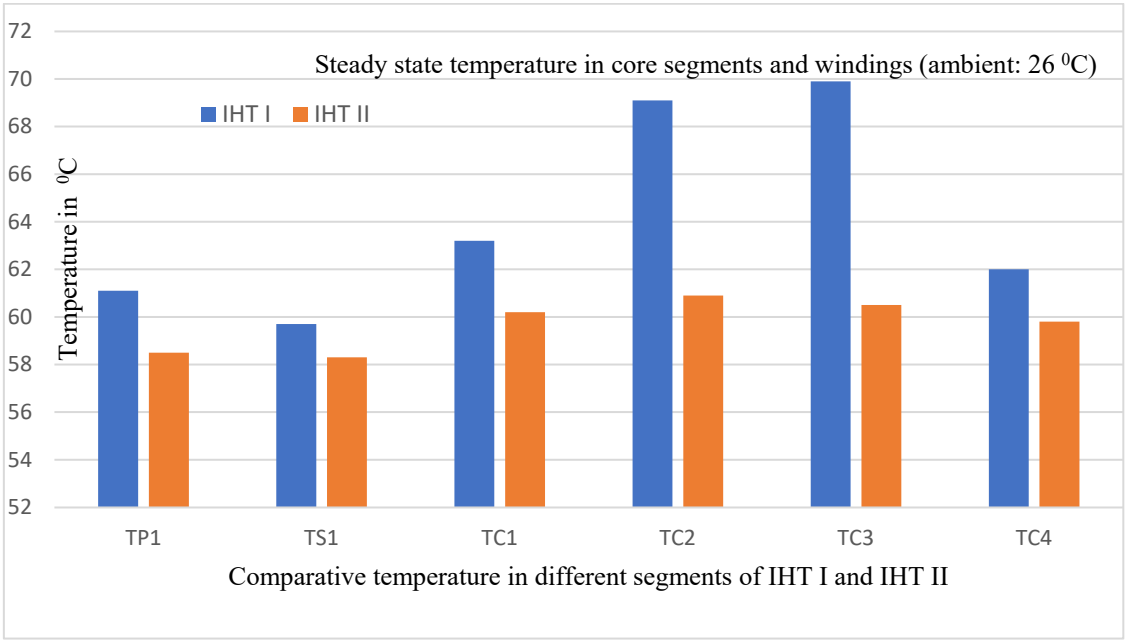

Figure 23. Compared to IHT I, the steady state temperature in different parts of IHT II was not only reduced, there was increased uniformity in maximum temperature in various parts of the mixed-core transformer.

5. Conclusions

The total power loss (i.e., core plus copper losses) in the majority of PETs would take place around a small core volume where the primary and secondary windings were overlaid. The surface area belonging to the rest of the core volume would remain exposed to the ambient environment. This article analyzed that the exposed surface area could be utilized effectively for heat transfer to the surrounding medium if the heat loss was easily channelized. The article proposed that a mixed-core configuration in the magnetic circuit could be used to achieve the goal. The idea was to replace the critical segment of the magnetic circuit having constrained heat conduction features by a geometrically compatible new core segment. The new segment would possess certain superior features, e.g., in core loss density, thermal conductivity, etc. To establish the compatibility of new core material, suitability factors were introduced for two different types of reluctance circuits. To validate the proposed idea, two transformers were built to cater two characteristically different applications. Initially, the magnetic compatibility of both the magnetic circuits under a worst-case operating condition were validated. Finally, both the transformers were put on prolonged load testing to comparatively validate their thermal performance. For both type of magnetic circuits, the superior thermal performance achieved during the heat run test

validated the proposed idea. The reduced hot spot temperature in core and copper meant that the capacity rating of mixed-core transformer could be upgraded.

Funding: This research received no external funding and there is no APC involved for the article. The article is submitted on invitation.

Acknowledgments: The author thanks Vijay Lotekar, Vaibhav Arde, Mangesh Waman and Bhavna Rahate of Electronics Devices Pvt. Ltd. for assistance during experiments.

Conflicts of Interest: The author declares that there is no conflict of interest.

References

1. Popović-Gerber, J.; Oliver, J.A.; Cordero, N.; Harder, T.; Cobos, J.A.; Hayes, M.; O'Mathuna, S.C.; Prem, E. Power electronics enabling efficient energy usage: Energy savings potential and technological challenges. *IEEE Trans. Power Electrons* **2012**, *27*, 2338–2353. [CrossRef]
2. Hurley, W.G.; Wolfle, W.H.; Breslin, J.G. Optimized transformer design: Inclusive of high-frequency effects. *IEEE Trans. Power Electrons* **1998**, *13*, 651–659. [CrossRef]
3. Mogorovic, M.; Dujic, D. Thermal modeling and experimental verification of an air cooled medium frequency transformer. In Proceedings of the 2017 19th European Conference on Power Electronics and Applications (EPE'17 ECCE Europe), Warsaw, Poland, 11–14 September 2017; pp. 1–9.
4. Paul, A.K. ZVZCS SRI guides optimal use of copper and core for air-cooled nanocrystalline transformer for induction heating. *IEEE Trans. Ind. Appl.* **2020**, *56*, 970–978. [CrossRef]
5. Ruiz, R.D.; Venegas, R.V.; Anaya, R.A.; Moreno, G.E.; Rodríguez, R.J. Design and prototyping medium frequency transformers featuring a nanocrystalline core for DC−DC converter. *Energies* **2018**, *11*, 2081. [CrossRef]
6. Liu, J.; Sheng, L.; Shi, J.; Zhang, Z.; He, X. Design of high voltage, high power and high frequency transformer in LCC resonant converter. In Proceedings of the 2009 Twenty-Fourth Annual IEEE Applied Power Electronics Conference and Exposition, Washington, DC, USA, 15–19 February 2009; pp. 1034–1038.
7. Shen, W.; Wang, F.; Boroyevich, D.; Tipton, C.W., IV. High-Density Nanocrystalline Core Transformer for High-Power High-Frequency Resonant Converter. *IEEE Trans. Ind. Appl.* **2008**, *44*, 213–222. [CrossRef]
8. Yao, P.; Jiang, X.; Xue, P.; Li, S.; Lu, S.; Wang, F. Design optimization of medium-frequency transformer for DAB converters with DC bias capacity. *IEEE J. Emerg. Sel. Top. Power Electron.* **2021**, *9*, 5043–5054. [CrossRef]
9. Shih, L.; Liu, Y.; Chiu, H. A novel hybrid mode control for a phase-shift full-bridge converter featuring high efficiency over a full-load range. *IEEE Trans. Power Electron.* **2019**, *34*, 2794–2804. [CrossRef]
10. Costinett, D.; Seltzer, D.; Maksimovic, D.; Zane, R. Inherent volt-second balancing of magnetic devices in zero-voltage switched power converters. In Proceedings of the 2013 Twenty-Eighth Annual IEEE Applied Power Electronics Conference and Exposition (APEC), Long Beach, CA, USA, 17–21 March 2013; pp. 9–15. [CrossRef]
11. Choi, J.M.; Byen, B.J.; Lee, Y.J.; Han, D.H.; Kho, H.S.; Choe, G.H. Design of leakage inductance in resonant DC−DC converter for electric vehicle charger. *IEEE Trans. Magn.* **2012**, *48*, 4417–4420. [CrossRef]
12. Ram, B.S.; Paul, A.K.; Kulkarni, S.V. Soft magnetic materials and their applications in transformers. *J. Magn. Magn. Mater.* **2021**, *537*, 168210. [CrossRef]
13. Kauder, T.; Hameyer, K. Performance factor comparison of nanocrystalline, amorphous and crystalline soft-magnetic materials for medium frequency applications. *IEEE Trans. Magn.* **2017**, *53*, 8401504. [CrossRef]
14. Jimenez, H.O. AC resistance Evaluation of Foils, Round and Litz Conductors in Magnetic Components. Master's Thesis, Chalmers University of Technology, Göteborg, Sweden, 2013.
15. Morched, A.; Marti, L.; Ottevangers, J. A high frequency transformer model for the EMTP. *IEEE Trans. Power Deliv.* **1993**, *8*, 1615–1626. [CrossRef]
16. Mu, M. High Frequency Magnetic Core Loss Study. Ph.D. Thesis, Virginia Polytechnic Institute and State University, Blacksburg, VA, USA, 2013.
17. Muhlethaler, J.; Beila, J.; Kolar, J.W.; Ecklebe, A. Core losses under the DC bias condition based on Steinmetz parameters. *IEEE Trans. Power Electron.* **2012**, *27*, 953–963. [CrossRef]
18. Rodriguez-Sotelo, D.; Rodriguez-Licea, M.A.; Araujo-Vargas, I.; Prado-Olivarez, J.; Barranco-Gutiérrez, A.I.; Perez-Pinal, F.J. Power losses models for magnetic cores: A review. *Micromachines* **2022**, *13*, 418. [CrossRef] [PubMed]
19. Venkatachalam, K.; Sullivan, C.R.; Abdallah, T.; Tacca, H. Accurate prediction of ferrite core loss with nonsinusoidal waveforms using only Steinmetz parameters. In Proceedings of the 2002 IEEE Workshop on Computers in Power Electronics, 2002. Proceedings, Mayaguez, PR, USA, 3–4 June 2002; pp. 36–41. [CrossRef]
20. Wang, Y.R. Modelling and Characterization of Losses in Nanocrystalline Cores. Ph.D. Thesis, University of Manchester, Manchester, UK, 2015.
21. Bahamani, M. Design and Optimization Considerations of Medium-Frequency Power Transformer in High-Power DC−DC Applications. Ph.D. Thesis, Chalmers University of Technology, Gothenberg, Sweden, 2016.

22. Bahmani, M.A.; Thiringer, T. Accurate evaluation of leakage inductance in high-frequency transformers using an improved frequency-dependent expression. *IEEE Trans. Power Electron.* **2015**, *30*, 5738–5745. [CrossRef]
23. Hurley, W.G.; Gath, E.; Breslin, J.G. Optimizing the AC resistance of multilayer transformer windings with arbitrary current waveforms. *IEEE Trans. Power Electron.* **2000**, *15*, 369–376. [CrossRef]
24. Zhao, H.; Eldeeb, H.H.; Zhang, Y.; Zhang, D.; Zhan, Y.; Xu, G.; Mohammed, O.A. An improved core loss model of ferromagnetic materials considering high-frequency and nonsinusoidal supply. *IEEE Trans. Ind. Appl.* **2021**, *57*, 4336–4346. [CrossRef]
25. Li, Z.; Yao, K.; Li, D.; Ni, X.; Lu, Z. Core loss analysis of Finemet type nanocrystalline alloy ribbon with different thickness. *Prog. Nat. Sci. Mater. Int.* **2017**, *27*, 588–592. [CrossRef]
26. Zhou, Y.; Qi, B.; Zheng, M.; Cong, B. A novel DC bias suppression strategy for single-phase full-bridge DC−DC arc welding converter. *Electronics* **2021**, *10*, 428. [CrossRef]
27. Kohama, T.; Tokimatsu, S.; Shimamori, H. Elimination of magnetic saturation due to fast dynamic response in DC−DC converter. In Proceedings of the INTELEC 2009—31st International Telecommunications Energy Conference, Incheon, Korea, 18–22 October 2009; pp. 1–6. [CrossRef]
28. Paul, A.K. Choice of control function in magnetically-coupled full bridge DC−DC power controller for arc welding: A practical approach. *J. Power Electron. Devices Compon.* **2022**, *2*, 100005. [CrossRef]
29. Paul, A.K. Emulating full load testing of air-cooled nanocrystalline IHT at zero power. *IEEE J. Emerg. Sel. Top. Ind. Electron.* **2022**, *3*, 725–732. [CrossRef]
30. Wang, H.; Blaabjerg, F. Power electronics reliability: State of the art and outlook. *IEEE J. Emerg. Sel. Top. Power Electron.* **2021**, *9*, 6476–6493. [CrossRef]
31. Nikolov, G.T.; Valchev, V.C. Nanocrystalline magnetic materials vs ferrites in power electronics. *Procedia Earth Planetory Sci.* **2009**, *1*, 1357–1361. [CrossRef]
32. Hilal, A.; Raulet, M.A.; Martin, C.; Sixdenier, F. A comparative study: Dynamic and thermal behavior of nanocrystalline and powder magnetic materials in a power converter application. *J. Electron. Mater.* **2015**, *44*, 3768–3776. [CrossRef]
33. Paul, A.K. Robust product design using SOSM for control of shielded metal arc welding (SMAW) process. *IEEE Trans. Ind. Electron.* **2016**, *63*, 3717–3724. [CrossRef]
34. Malesani, L.; Mattavelli, P.; Rossetto, L.; Tenti, P.; Marin, W.; Pollmann, A. Electronic welder high frequency resonant converter. *IEEE Trans. Ind. Appl.* **1995**, *31*, 273–279. [CrossRef]
35. Ruiz-Robles, D.; Moreno-Goytia, E.L.; Venegas-Rebollar, V.; Salgado-Herrera, N.M. Power density maximization in medium frequency transformers by using their maximum flux density for DC–DC converters. *Electronics* **2020**, *9*, 470. [CrossRef]
36. Paul, A.K. Structured protection measures for better use of nanocrystalline cores in air-cooled medium-frequency transformer for induction heating. *IEEE Trans. Ind. Electron.* **2021**, *68*, 3898–3905. [CrossRef]
37. Meziane, B.; Zeroug, H. Improved efficiency determination for a PLL-controlled series resonant inverter for induction metal surface hardening. In Proceedings of the 2015 IEEE Industry Applications Society Annual Meeting, Addison, TX, USA, 18–22 October 2015; pp. 1–8.
38. Plesca, A. Considerations about maximum temperature of toroidal transformers in steady-state conditions. *J. Adv. Therm. Sci. Res.* **2020**, *7*, 22–29. [CrossRef]
39. Purushothaman, S.; de Leon, F. Heat-transfer model for toroidal transformers. *IEEE Trans. Power Deliv.* **2012**, *27*, 813–820. [CrossRef]
40. Lefevre, G.; Chazal, H.; Ferrieux, J.P.; Roudet, J. Application of Dovvell method for nanocrystalline toroid high frequency transformers. In Proceedings of the 2004 IEEE 35th Annual Power Electronics Specialists Conference (IEEE Cat. No.04CH37551), Aachen, Germany, 20–25 June 2004; Volume 2, pp. 899–904. [CrossRef]
41. Petkov, R. Optimum design of a high-power, high-frequency transformer. *IEEE Trans. Power Electron.* **1996**, *11*, 33–42. [CrossRef]
42. Jaritz, M.; Biela, J. Analytical model for the thermal resistance of windings consisting of solid or litz wire. In Proceedings of the 2013 15th European Conference on Power Electronics and Applications (EPE), Lille, France, 2–6 September 2013; pp. 1–10. [CrossRef]
43. Kącki, M.; Rylko, M.S.; Hayes, J.G.; Sullivan, C.R. Magnetic material selection for EMI filters. In Proceedings of the 2017 IEEE Energy Conversion Congress and Exposition (ECCE), Cincinnati, OH, USA, 1–5 October 2017; pp. 2350–2356. [CrossRef]